THE JOURNAL OF PHYSICAL CHEMISTRY B

Article

pubs.acs.org/JPCB

Modeling Aggregation of Ionic Surfactants Using a Smeared Charge Approximation in Dissipative Particle Dynamics Simulations

Runfang Mao, Ming-Tsung Lee, Aleksey Vishnyakov, and Alexander V. Neimark*

Department of Chemical Engineering, Rutgers, the State University of New Jersey, 98 Brett Road, Piscataway, New Jersey 08854, United States

Supporting Information

ABSTRACT: Using dissipative particle dynamics (DPD) simulations, we explore the specifics of micellization in the solutions of anionic and cationic surfactants and their mixtures. Anionic surfactant sodium dodecyl sulfate (SDS) and cationic surfactant cetyltrimethylammonium bromide (CTAB) are chosen as characteristic examples. Coarse-grained models of the surfactants are constructed and parameterized using a combination of atomistic molecular simulation and infinite dilution activity coefficient calibration. Electrostatic interactions of charged beads are treated using a smeared charge approximation: the surfactant heads and dissociated counterions are modeled as beads with charges distributed around the bead center in an implicit dielectric medium. The proposed models semi-quantitatively describe self-assembly in solutions of SDS and CTAB at various surfactant concentrations and molarities of added electrolyte. In particular, the model predicts a decline in the free surfactant concentration with the increase of the total surfactant loading, as well as characteristic aggregation transitions in single-component surfactant solutions caused by the addition of salt. The calculated values of the critical micelle concentration reasonably agree with experimental observations. Modeling of catanionic SDS−CTAB mixtures show consecutive transitions to worm-like micelles and then to vesicles caused by the addition of CTAB to micellar solution of SDS.

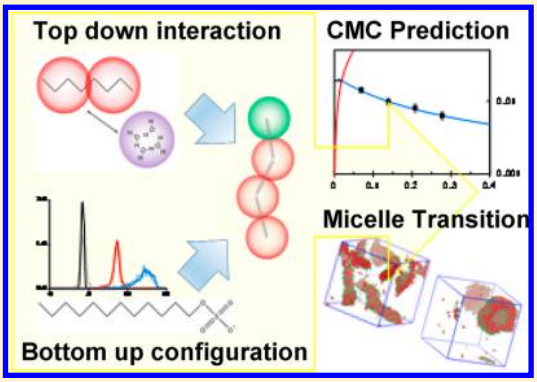

1. INTRODUCTION

Dissipative particle dynamics (DPD) simulations[1] have become a powerful tool for modeling soft matter systems on the spatial and temporal scales that cannot be accessed on the quantum or atomistic levels. In the common implementations of DPD, the molecule of interest is dissected into fragments of approximately equal volume. The atoms of each fragment are lumped together and represented as spherical quasiparticles ("beads") that interact via short-range soft-core repulsive potentials. This approach provides a superb computational efficiency. The price to pay for that is a crudeness of models that limits the range of systems and phenomena, for which DPD simulations are capable of quantitative predictions. Traditional applications of DPD include self-assembled nonionic systems (such as micellar solutions, block copolymers, lipid bilayers),[2−7] while the attempts to extend the soft-core models to the systems, where long-range electrostatic interactions play a key role, are quite sparse.

Technical problems with treating electrostatic forces in DPD originate from divergence of the Coulomb potential at small distances between the beads, which may overlap in soft-core models. A popular approach to avoid apparent difficulties of accounting for explicit long-range electrostatic interactions in DPD consists of their replacement by effective short-range potentials.[8−10] This method was also used in the mesoscale dynamic density functional theory.[11] However, this approach is based on the Donnan approximation, which is only valid at very high ionic strength.[12] To enable explicit charge simulations, Groot[13] introduced a smeared charge model, where, in contrast to the point charge model standard in molecular dynamics (MD), the charge is distributed around the bead center. Linear,[13] Slater-type exponential,[14] Gaussian-type,[15] and Bessel-type[16] distributions of charge density have been considered in the literature. The smeared charge models imply two main assumptions: (1) charge distribution is isotropic and spherically symmetric that rarely corresponds to the actual structure of complex cations or anions of ionic surfactants and polyelectrolytes; (2) charges interact in an isotropic medium characterized by a uniform dielectric constant ε, that means that the local environment does not affect the pairwise electrostatic interactions. The smeared charge models have been applied to complex systems and phenomena, such as bulk electrolytes, individual polyelectrolyte molecules in electrolyte solutions, polymer brushes, polyelectrolyte translocation though narrow pores, hydrated polyelectrolyte membranes, peptides, and even dendrimer interactions with lipid bilayers.[13,14,17−21] Nevertheless, the predictive capabilities of the soft-core smeared charge models remain unexplored.

Received: June 12, 2015
Revised: July 23, 2015

DOI: 10.1021/acs.jpcb.5b05630
J. Phys. Chem. B XXXX, XXX, XXX−XXX

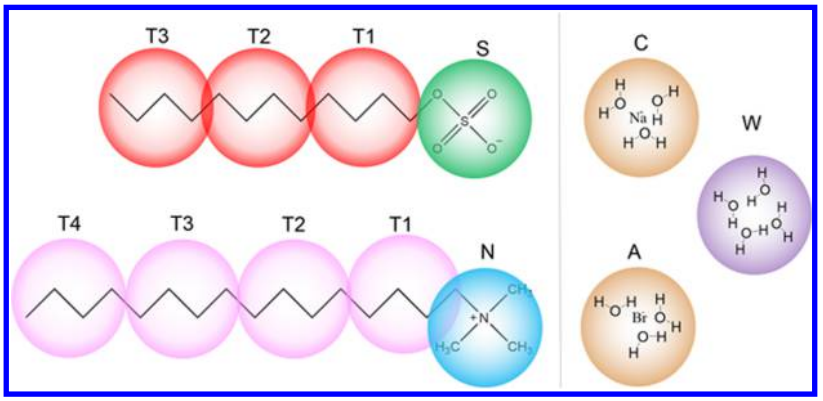

Figure 1. Schematics of the coarse-grained models of SDS and CTAB. SDS (sodium dodecyl sulfate) is represented as a chain of three tail T (T1−T3) beads and one anionic head bead S. CTAB (cetyltrimethylammonium bromide) is represented by four tail T beads (T1−T4) and one cationic head bead N. Counterions hydrated by three water molecules are represented by cation C and anion A beads. Water bead W contains four water molecules.

Various charge distribution functions used in simulations and their influence on the thermodynamics and structure of electrolytes are yet to be examined. Warren and Vlasov[16] advise to choose the type and parameters of the charge distribution function to maximize the computational efficiency rather than to match particular thermodynamic or structural properties. Even on a qualitative level, the capabilities of DPD with smeared charges have not been rigorously tested, and the range of phenomena they are able to describe on a quantitative basis remains unclear.

The difficulties in the treatment of electrostatic interactions are not specific to DPD and are also present in other coarse-grained techniques like MD, Brownian dynamics (BD), and lattice Monte Carlo (MC) simulations. It is worth noting that the MC technique was recently successfully employed in simulation of micellization in solutions of ionic surfactants providing quantitative agreement with the experiment. Cheong and Panagiotopoulos[22] modeled sodium dodecyl sulfate (SDS) solutions with the lattice MC technique using different volumes of head and tail beads and explicit charges. The model reproduced a nontrivial dependence of the critical micelle concentration (CMC) on the temperature with a characteristic minimum. At the same time, the absolute value of CMC was underestimated by approximately an order of magnitude at room temperature. In the lattice MC simulation of Jusufi et al.,[23] the coarse-grained interaction parameters for the head and counterion beads were obtained by matching structural quantities of explicit solvent MD and implicit solvent MC systems, while the parameters of hydrophobic attraction between the tail beads were matched to experimental CMC via histogram reweighting MC simulations. The authors transferred the obtained potentials to similar surfactants with different counterions and tail length and obtained reasonable agreement with experimental CMC and the aggregation number N_{ag}.

DPD studies of ionic surfactants using charge smearing have been quite limited. Very recently, Posel et al.[17] tested the pH-dependent self-assembly of diblock copolymer using a Slater-type smearing charge distribution. In order to model the dependence of ionization on pH, the authors varied the charge of the hydrophilic block according to dissociation constant (a similar approach was used earlier in DPD simulations of peptides[20]). The authors found a clear transition from dissolved to associated state occurred at a narrow pH range above pK_a that is in agreement with experiment.[24] The parameters obtained were then applied in a systematic study of electrostatic assembly of diblock copolymer with opposite charges ($A_n^-B_n$ and $A_n^+B_n$).[25] With a very short smearing length ($\lambda = 0.2$), the aggregation behavior of compatible copolymer and the influence of counterion were qualitatively reproduced. However, we are not aware of systematic studies of micellization of ionic surfactants using the smeared charge models and attempts to use DPD to account for the salt effect and the interactions of cationic and anionic surfactants in catanionic mixtures.

In this paper, we examine the capabilities of DPD models with smeared charge electrostatic potentials for modeling ionic surfactant self-assembly. As a case study, we consider the specifics of micellization in single component and binary solutions of two common surfactants: sodium dodecyl sulfate (SDS, Figure 1a) and cetyltrimethylammonium bromide (CTAB, Figure 1b). Section 2 is devoted to the description of the DPD methodology along with the coarse-grained model and force field development. In section 3, we present the results of DPD calculations of the CMC. Micelle sizes in single-component surfactant solutions are considered in section 4. The effect of charge screening caused by the addition of salt is described in section 5. Section 6 explores the specifics of micellar aggregation in the mixtures of cationic and anionic surfactants. The significance of the proposed approach and its limitations are summarized in section 7.

2. SYSTEMS, METHODS, AND SIMULATION DETAILS

2.1. Coarse-Graining of Surfactants and Forces between Coarse-Grained Particles. The conventional DPD methodology requires the use of the coarse-grained beads of the same size. This restriction dictates the choice of the dissection of the surfactant molecules considered in this study (SDS and CTAB) into the fragments of approximately similar size: hydrophobic tail T beads lumps together four methyl/methylene groups, so that the size of the hydrophobic tail beads conveniently equals those of hydrophilic heads. The latter are denoted as S bead for the sulfate head of SDS and N bead for the trimethylammonium head bead of CTAB, as shown in Figure 1. Water is modeled with W beads, and each W bead contains four water molecules ($N_W = 4$) in order to match the volume of the tail fragment according to the liquid densities of water and octane.[26] In previous simulations of ionic systems, the coarse graining level was varied from $N_W = 2$ (ref

DOI: 10.1021/acs.jpcb.5b05630
J. Phys. Chem. B XXXX, XXX, XXX−XXX

20) to N_W = 11 (ref 27). N_W = 4 chosen in this work was previously applied in simulations of hydrated Nafion and is far from the limit, where artificial freezing of DPD solvent[28] can be observed. Cation C and anion A beads represent counterions and the ions of added salt; each of them effectively represents an ion atom hydrated by three water molecules. They are modeled as "charged water" beads,[13,18] with the same mass and conservative parameters as W beads but bearing either positive $+e$ or negative $-e$ charge. Each tail bead equals four methyl/methylene groups of the alkyl chain.[29] SDS and CTAB molecules have three and four T beads, respectively.

We employed the conventional DPD scheme with the particles interacting via pairwise conservative soft repulsive $\mathbf{F}_{ij}^{(C)}(\mathbf{r}_{ij})$, bond $\mathbf{F}_{ij}^{(B)}(\mathbf{r}_{ij})$, and electrostatic $\mathbf{F}_{ij}^{(E)}(\mathbf{r}_{ij})$ forces, as well as random $\mathbf{F}_{ij}^{(R)}(\mathbf{r}_{ij})$ and velocity dependent drag $\mathbf{F}_{ij}^{(D)}(\mathbf{r}_{ij}, \mathbf{v}_{ij})$ forces:

$$\mathbf{F}_{ij}(\mathbf{r}_{ij}) = \mathbf{F}_{ij}^{(C)}(\mathbf{r}_{ij}) + \mathbf{F}_{ij}^{(B)}(\mathbf{r}_{ij}) + \mathbf{F}_{ij}^{(E)}(\mathbf{r}_{ij}) + \mathbf{F}_{ij}^{(R)}(\mathbf{r}_{ij}) + \mathbf{F}_{ij}^{(D)}(\mathbf{r}_{ij}, \mathbf{v}_{ij}) \quad (1)$$

All beads are assigned an equal effective diameter R_c. The soft repulsion force $\mathbf{F}_{ij}^{(C)}$ acts between overlapping beads: $\mathbf{F}_{ij}^{(C)}(\mathbf{r}_{ij}) = a_{IJ}(1 - r_{ij}/R_c)\mathbf{r}_{ij}/r_{ij}$ at $r < R_c$, $\mathbf{F}_{ij}^{(C)}(\mathbf{r}_{ij}) = 0$ at $r \geq R_c$, where a_{IJ} is the repulsion parameter specific to a given bead pair of type I and J. Following the standard approach to DPD simulations of self-assembly,[7] the intracomponent repulsion parameters a_{II} between beads of the same type are set equal, irrespective to the bead type. The beads are tightly packed with a substantial overlap. We accepted the reduced bead packing density of $\rho R_c^3 = 3$, common in DPD simulations.[7]

The Langevin thermostat is maintained by random and drag forces, acting between overlapping beads along the vector $\mathbf{r}_{ij}$ connecting the bead centers. The random force $\mathbf{F}_{ij}^{(R)}$ that accounts for thermal fluctuations is taken proportional to the conservative force: $\mathbf{F}_{ij}^{(R)}(\mathbf{r}_{ij}) = \sigma w^R(r_{ij})\theta_{ij}(t)\mathbf{r}_{ij}$, where $\theta_{ij}(t)$ is a randomly fluctuating in time variable with Gaussian statistics. The drag force is velocity-dependent: $\mathbf{F}_{ij}^{(D)}(\mathbf{r}_{ij}, \mathbf{v}_{ij}) = -\gamma w^D(r_{ij})(\mathbf{r}_{ij}*\mathbf{v}_{ij})$, where $\mathbf{v}_i$ and $\mathbf{v}_j$ are the current velocities of the particles, and $\mathbf{v}_{ij} = \mathbf{v}_j - \mathbf{v}_i$. We assume the common relationships between the drag and random force weighting functions $w(r)$ and parameters σ and γ that determine the levels of energy fluctuation and dissipation $w^D(r) = [w^R(r)]^2 = (1 - r/R_c)^2$ at $r < R_c$ and $\sigma^2 = 2\gamma kT$. This allows a constant temperature to be maintained in the course of simulation via the Langevin thermostat. We assumed γ = 4.5, a common value used in DPD simulations of water.[7]

The chain beads are connected by either harmonic or FENE bonds that $\mathbf{F}_{ij}^{(B)}(\mathbf{r}_{ij}) = K_b(r_0 - r_{ij})/(1 - ((r_{ij} - r_0)^2/r_m^2))\mathbf{r}_{ij}/r_{ij}$, where K_b is the bond rigidity, r_0 is the equilibrium bond length, and r_m is the maximum bond length. Following our recent papers,[29,30] in addition to this nearest neighbor (1−2) bond, we introduced the second neighbor (1−3) harmonic or FENE bonds in order to control the chain flexibility. As shown below, this approach provides for the systems studied good agreement between the conformation of atomistic and coarse grained chains without invoking a torsion (1−4) potential.

The electrostatic interactions are modeled using the smeared charge approach with the Slater-type charge density distribution with an exponential decay,[14] $f(r) = (q/\pi\lambda^3)\exp(-(2r/\lambda))$, where λ is the effective smearing radius. The electrostatic force $\mathbf{F}_{ij}^{(E)}$ between charged particles i and j in eq 1 is expressed as

$$\mathbf{F}_{ij}^{(E)}(\mathbf{r}_{ij}) = \frac{e^2 q_i q_j}{4\pi kT\varepsilon_0\varepsilon_r R_C r_{ij}^2}[1 - \exp(-2R_C r_{ij}/\lambda r_{ij})(1 + 2R_C r_{ij}/\lambda(1 + R_C r_{ij}/\lambda))]\frac{\mathbf{r}_{ij}}{r_{ij}} \quad (2)$$

At long range, the electrostatic interaction of smeared charges (eq 2) reduces to the Coulomb potential and the standard Ewald summation[31] is used to account for the periodic boundary conditions. The choice of the smearing radius $\lambda = 0.25R_c$ for all charged beads was made due to technical reasons, as described in the Supporting Information, section S2.

2.2. Parameterization of the DPD Model. Accurate parametrization of coarse-grained interaction potentials from independent data taken either from experiments or from quantum mechanical and atomistic simulations is a prerequisite for constructing DPD models with predictive capabilities. In our recent papers,[20,29] we suggested a strategy for determining the intracomponent and intercomponent repulsion and bond parameters. Following this strategy, we first determine the intracomponent repulsion parameter from the solvent compressibility at the given coarse-graining level (N_W = 4), which is dictated by the chosen dissection of the molecules into beads of equal size (Figure 1). The intracomponent repulsion parameter is set the same for all bead types $a_{WW} = a_{TT} = a_{HH} = a_{CC} = 106.5\ k_BT/R_c$, the value found from the water compressibility at N_W = 4.[20] This value sets the benchmark for determining the intercomponent repulsion parameters from the correlation of the infinite dilution activity coefficients (IDAC) in binary solutions of reference compounds.

The bond parameters are determined from the correlation of the chain rigidity of reference compounds on the atomistic and coarse-grained level. The bond parameters for tail−tail bead interactions in the alkyl chain are found from the analysis of conformations of hexadecane presented on the coarse grained level as a tetramer of T beads. Using the CHARMM-27 force field,[32] we performed atomistic MD simulations of pure hexadecane. The details of the MD simulation are described in the Supporting Information, section S1. Each molecule was dissected into four fragments (four CH_x groups each), and the probability distributions of the intramolecular distances between the centers of mass of each fragment were calculated. In parallel, we conducted DPD simulations of pure tetramers melting with $a_{TT} = 106.5\ k_BT/R_c$ at similar conditions and fitted the nearest neighbor and second neighbor bond parameters to reproduce the distributions of distances between first, second, and third neighboring beads obtained in atomistic separations. The results shown in Figure 2 confirm that the proposed coarse-grained model is able to reproduce accurately the alkyl chain rigidity without employing additional torsional potentials. The potential parameters are given in Table 1.

In the next step, we evaluate the repulsion parameter a_{WT} between T and W beads from the mutual solubilities of octane and water.[29] Octane molecule is presented as a T−T dimer with the repulsion parameter a_{TT} and the FENE bond potential determined above for the alkyl chain. a_{WT} is calculated from the best match between the solubility of the DPD model of octane in the DPD model of water and the experimental solubility. The a_{WT} dependence of the IDAC of the T−T dimer in the bath of water W beads is obtained from the MC simulation using the Widom test particle insertion method.[33] This dependence serves as the calibration curve to find the value

DOI: 10.1021/acs.jpcb.5b05630
J. Phys. Chem. B XXXX, XXX, XXX−XXX

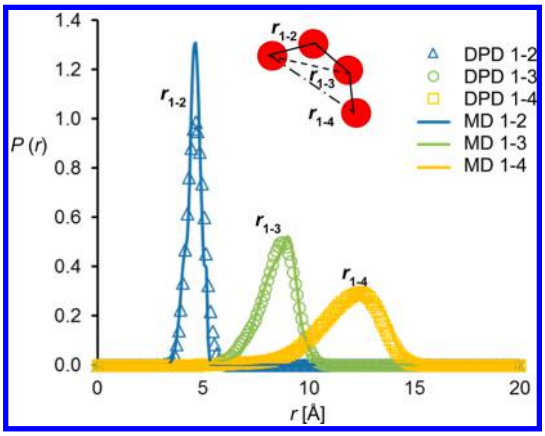

Figure 2. Fitting the bond rigidity in the DPD model of liquid hexadecane $C_{16}H_{34}$ to the results of atomistic MD simulations at T = 298 K. The distribution of distances between the chain DPD beads separated by one (1−2), two (1−3), and three (1−4) nearest-neighbor bonds are matched to the distributions of distances between the centers of mass of the corresponding fragments of the atomistic chain, each of which contains four CH_3 or CH_2 groups. The solid lines are obtained by MD simulations and open symbols by DPD simulations.

of a_{WT} that provides the experimental IDAC of octane in water. The procedure is repeated to determine the IDAC of water in octane. In the latter simulation, the bead density in the system is set at 3.05 in order to equalize the pressures in the water and octane baths. The value of a_{WT} obtained from the water-in-octane solubility somewhat differs from that obtained from the octane-in-water solubility; the average of these two values is taken as the tail−water repulsion parameter, a_{WT} = 129.9 k_BT/R_c, for further DPD simulations. It is worth noting that the parameters for T−T bond and W−T repulsion in this work slightly differ from those used in ref 29 due to the refined calibration of the bond parameters (Figure 2). They also differ from the Δa_{TW} calculated from the Flory−Huggins parameter,[29] since the Flory−Huggins model implies a fully flexible chain with the bead diameter comparable to the persistent length. In the case of the relatively small beads considered here, this assumption may alter the sizes and shapes of the simulated micelles, even when the CMC is correctly reproduced.[29]

The surfactant heads are assumed hydrophilic $a_{WS} = a_{WN} = a_{SN}$ = 106.5 k_BT/R_c, and the head−tail parameters were assigned approximately, since strict parametrization techniques for charged beads are still lacking in the literature. Sulfate−alkyl S−T interactions were made strongly unfavorable, a_{TS} = 136.5 k_BT/R_c, and alkylamine−alkyl N−T interactions, about half as unfavorable as T−W interactions, a_{TN} = 111.5 k_BT/R_c. The parameters for 1−2 and 1−3 bonds are found similarly to those for T−T bonds. We simulated dilute aqueous solutions of SDS and CTAB in atomistic MD simulations and fitted the DPD bond parameters to match the distribution of interbead distances in the coarse-grained surfactant molecule to the MD results. Figure 3 shows a good match of the surfactant conformations in DPD and MD simulations. The interaction parameters are given in Table 1.

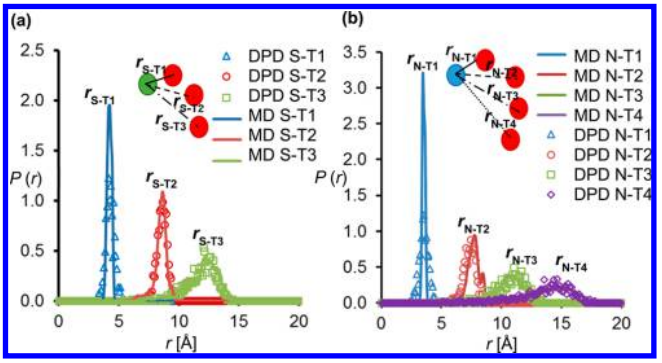

Figure 3. Fitting the parameters for head−tail bonds S−T1, S−T2, N−T1, and N−T2 in the DPD model to the results of atomistic MD simulations of SDS and CTAB in dilute aqueous solution at T = 298 K. The bead denotations correspond to Figure 1. DPD distributions of distances between the beads are matched to the distributions of distances between the centers of mass of the corresponding fragments (Figure 1). The solid lines are obtained by MD simulations and open symbols by DPD simulations.

2.3. DPD Simulation Details. The DL_MESO package[34] is employed for DPD simulations of micellization. All simulations are performed in periodic cubic boxes. The box size is varied from 30 to 40 R_c in order to collect sufficient statistics. The surfactant volume fraction ϕ is varied from 0.02

Table 1. Repulsion and Bond Parameters of the DPD Model[a]

Repulsion Parameters							
bead type	fragment	W	T	S	N	C^+	A−
W	$4H_2O$	106.5					
T	$(CH_x)_4$	129.9	106.5				
S	$-OSO_3$	106.5	136.5	106.5			
N	$-N(CH_3)_3^+$	106.5	111.5	106.5	106.5		
C^+	$Na(H_2O)_3^+$	106.5	129.9	106.5	106.5	106.5	
A	$Cl/Br(H_2O)_3$	106.5	129.9	106.5	106.5	106.5	106.5

Bond Parameters					
bond type	bead type	K_b/k_BT	r_0/R_c	r_m/R_c	
1−2	T−T	280	0.605	2.0	
	T1−S	300	0.5	∞	b
	T1−N	200	0.4	∞	b
1−3	T−(T)−T	20	1.5	4.0	
	T2−(T1)−N	150	1.3	∞	b
	T2−(T1)−S	120	1.1	∞	b

[a]Short-range repulsion parameters a_{IJ} are given in k_BT/R_c units. [b]Harmonic bond.

DOI: 10.1021/acs.jpcb.5b05630
J. Phys. Chem. B XXXX, XXX, XXX−XXX

to 0.08. For all simulations, the time step δt is set equal to $0.02(R_c^2 m_W/k_B T)^{1/2}$, where m_W is the mass of water bead and the friction parameter γ is set to 4.5 in order to keep temperature deviation under 1%. The length of each simulation was 2×10^6 steps; half of that was discarded for equilibration. Configurations are dumped to a trajectory file every 2000 steps after equilibration for processing and analysis. After the equilibration is complete, the number of free surfactant molecules and the average micelle size fluctuate around their average values; however, significant alterations of the overall morphology are observed (Supporting Information, section S3).

3. SELF-ASSEMBLY IN SINGLE-COMPONENT SURFACTANT SOLUTIONS. CRITICAL MICELLE CONCENTRATION

Aggregation of surfactant is characterized using the geometrical criteria employed in ref 29. Two surfactant molecules are assumed to belong to the same aggregate if any two of their tail beads overlap. If an aggregate contains more than a certain threshold n_{mic} of surfactant molecules, it is counted as a micelle. If a surfactant molecule belongs to a cluster containing less than n_{mono} surfactant molecules, it is assumed to be part of the "free surfactant". Aggregation is considered as complete and equilibrium reached when the free surfactant concentration stabilizes and becomes practically insensitive to the choice of n_{mono} and n_{mic} within reasonable limits. A detailed discussion of choosing n_{mono} and n_{mic} can be found in ref 29.

Figure 4 shows the probability of a surfactant molecule to belong to an aggregate of size N in CTAB and SDS aqueous solutions of different concentration. The difference between micelles and small short-living aggregates is very clear for sufficiently high concentrations. On the basis of these distributions, we used $n_{mono} = 5$ and $n_{mic} = 20$ for SDS and $n_{mono} = 3$ and $n_{mic} = 8$ for CTAB in order to calculate the free surfactant concentration and the micelle size. At a small surfactant volume fraction of $\phi = 0.02$, there is no clear boundary to distinguish between the aggregated and free surfactant molecules, since the probability decreases almost monotonically with the cluster size. This is probably related to an insufficient system size.

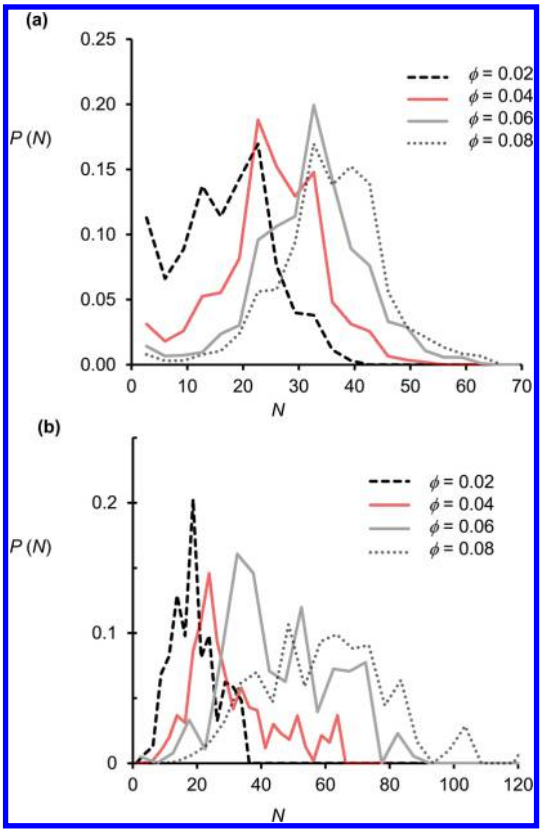

Figure 4. Probability of a surfactant molecule to belong to an aggregate of given size N in solutions of SDS (a) and CTAB (b) of different total surfactant volume fraction.

The dependence of the free surfactant concentration C_f on the total surfactant concentration C_T is shown in Figure 5. The concentrations are given in mol/L rather than in volume fractions in order to compare with relevant theoretical equations and experimental data, and calculated as $C = n/(N_A L^3 R_c^3)$, where n is the number of surfactant molecules (n_{total} or n_{free}) in the box. n_{free} includes surfactants in all aggregates smaller than n_{mono}, while n_{total} is the number of total surfactant molecules in the system. N_A is Avogadro's number, and L is the box size in R_c. The volume fraction ϕ is calculated as the ratio of the total number of surfactant beads excluding counterions to the total number of beads in the system. The simulation results are shown in Figure 5. Below the CMC when micelles are absent, $C_f = C_T$. As the CMC is reached, the dependence of C_f on C_T abruptly changes. In contrast to nonionic surfactants, the formation of micelles leads to a decrease of the free surfactant concentration C_f as the surfactant total surfactant concentration increases (when $C_T > C_{CMC}$). For nonionic surfactants, C_f slowly increases with ϕ and approaches a plateau that can be identified with the CMC with a reasonable accuracy.[29] The decline of the free surfactant concentration above the CMC is caused by electrostatic interactions between micelles and free surfactant molecules. This phenomenon is specific to ionic surfactants and was observed experimen-

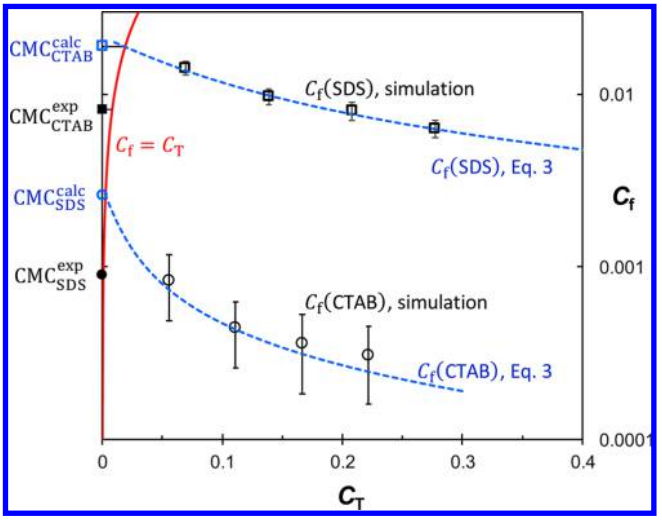

Figure 5. Dependence of the free surfactant concentration C_f on the total surfactant concentration C_T for SDS and CTAB. Results of DPD simulations are shown by open symbols. Dashed lines are the dependence of the free surfactant concentration C_f of SDS and CTAB according to eq 3. The red line represents the linear relationship $C_f = C_T$ that is held in uniform solutions below the CMC. The CMC is estimated as the intersection between the "C_f–C_T" curve and dashed lines obtained from eq 3. The CMCs^{exp} are shown in filled symbols (experimental data is from ref 39).

DOI: 10.1021/acs.jpcb.5b05630
J. Phys. Chem. B XXXX, XXX, XXX–XXX

tally[35,36] and predicted theoretically[37,38] and by MD simulations.[22,38]

In order to estimate the CMC from the calculated values of C_f, we employ the semiempirical theory of Sanders et al.,[37,38] where the relation between free surfactant concentration C_f and total surfactant concentration C_T is expressed as

$$\log(C_f) = (1 + \alpha)\log(C_{CMC}) - \alpha \log\left(\frac{(1-\alpha)(C_T - C_f) + C_f}{1 - VC_T}\right) \quad (3)$$

V is the molar volume of surfactant, and the units of C_T, C_f, and C_{CMC} are in mol/L.

The parameter α is the degree of association of the counterions with the head groups of the surfactants forming the micelles, which means that an aggregate consisting of N surfactant molecules has N head beads and αN counterions and bears a charge of $\pm(1 - \alpha)N$.[38] The conventional DPD model cannot describe a dissociation/association of ionic pairs, and even the criteria of association are very hard to establish. We therefore treat both the CMC and α as adjustable parameters. Their values were determined from the best fit of C_f (C_T) dependence given by eq 3 to the C_f values obtained in our DPD simulations.[37,40] The results are shown in Figure 5. For SDS, agreement between eq 3 and the DPD results is obtained at α = 0.73 and a CMC of 19 mM. Surprisingly, the obtained α is very close to the experimental association degree used in ref 38. The calculated CMC exceeds the experimental value of 8.2 mM by a factor of 2.4. This (dis)agreement is acceptable given the state of the art in DPD simulations of ionic compounds, as we discuss in section 7. The accuracy of the DPD results for CTAB does not allow fitting both α and CMC: very low C_f and higher C_T results in a high relative error (Figure 5). We opted to use the experimental value of α = 0.78 and obtained a CMC of 2.6 mM, which is also somewhat higher than the experimental value[39] but yet reasonable given the accuracy of both simulations and experiments.

4. MICELLE SIZE

The surfactant aggregate size distributions given in Figure 4 are in general unimodal with well-defined maxima that is typical for spherical micelles. At higher concentrations of CTAB, a small fraction of elongated micelles is also observed. From these distributions, we calculated the aggregation number N_{ag} (that is, the average number of surfactant molecules in a micelle). Dependence of the aggregation number on the surfactant volume fraction is shown in Figure 6. The micelles grow with the total surfactant concentration, which is a well-established phenomenon in surfactant solutions. However, the micelles found in DPD simulations are 2−3 times smaller than those experimentally observed. For example, the experimental aggregation number in 0.05 M SDS solution is around N_{ag} = 65,[39,41] while we obtained a value around 30 at ϕ = 0.04 (approximately in 0.14 M SDS solution). CTAB forms somewhat larger micelles compared to SDS. This is consistent with the experimental results, for the CTAB molecule is longer than SDS. The micelle surface area of CTAB is greater than that of SDS micelle, so CTAB micelle can accommodate more head groups. Noteworthy, the experimental values of the aggregation number N_{ag} reported for the same system vary with the method used for its determination,[37,42,43] which makes the correlation of simulated and experimental data more difficult.

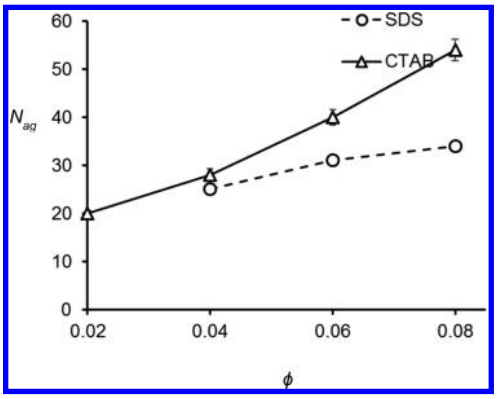

Figure 6. Dependence of the aggregation number N_{ag} on the surfactant volume fraction ϕ for SDS and CTAB. The system size is 40 × 40 × 40R_c^3.

5. SALT EFFECT

Addition of extra electrolyte to the system causes the charge screening effect on the micellization of ionic surfactant. As the ionic strength of the solution increases, the Debye length decreases, which reflects weakening the long-range electrostatic effects in the solution. Screening of electrostatic interactions changes the micelle size and shape: the micelles become larger and tend to merge into worm-like, cylindrical aggregates. The concentration of surfactant, at which the transition to worm-like aggregates occurs, is defined as the critical aggregation concentration (CAC). Addition of salt lowers the surfactant CAC and causes an aggregation transition in solutions of ionic surfactants that is well studied in the literature.

To demonstrate the ability of the proposed DPD model to reproduce the salt effect, we perform DPD simulations with SDS in a model 1:1 C^+A^- salt solution, effectively mimicking NaCl. This system was thoroughly studied in the literature both experimentally and with semiatomistic MD simulations.[44−46] The surfactant volume fraction is fixed at ϕ = 0.04, and the box size is L = 30 R_c. To increase the salt concentration, we replace water beads by the hydrated ion beads C^+ and A^- to achieve a salt concentration of 0.5, 1, 1.5, and 2 M.

Figure 7 shows equilibrated configurations of SDS at different salt concentrations. Addition of salt increases N_{ag} from 26, observed in pure surfactant, to 47, obtained in 0.5 M salt solution. Nevertheless, the micelles mostly retain a spherical shape, despite an increased size. This observation qualitatively agrees with experiments. However, the simulated micelles are consistently smaller than the ones reported in experiments, where the average size is 135 in 0.5 M electrolyte solution.[45] As the salt concentration increases, the micelles grow further and the aggregation number continually increases up to 133 in 2.0 M electrolyte. The micelles change in shape to larger worm-like micelles as the salt concentration increases to 1 M (Figure 7b). The micelle size distribution changes along with the distribution of the asphericity factors that is a quantitative measure of the departure from spherical symmetry of micelles.[47] The asphericity factor A is obtained from the gyration tensor $\mathbf{S}$ calculated for each individual micelle: $S_{ij} = (1/N)\sum_{l=1}^{N}(S_{il} - S_i^{CM})(S_{jl} - S_j^{CM})$, where S_i^{CM} stands for the center of mass coordinate (i denotes x, y, or z). After three eigenvalues R_1^2, R_2^2, and R_3^2 of the gyration tensor are obtained, the asphericity factor is calculated as $A = (1/2)R_g^4[(R_1^2 - R_2^2) + (R_1^2 - R_3^2) + (R_3^2 - R_2^2)]$, where $R_g^2 = R_1^2 + R_2^2 + R_3^2$ is the radius of gyration. The asphericity factor is 0

DOI: 10.1021/acs.jpcb.5b05630
J. Phys. Chem. B XXXX, XXX, XXX−XXX

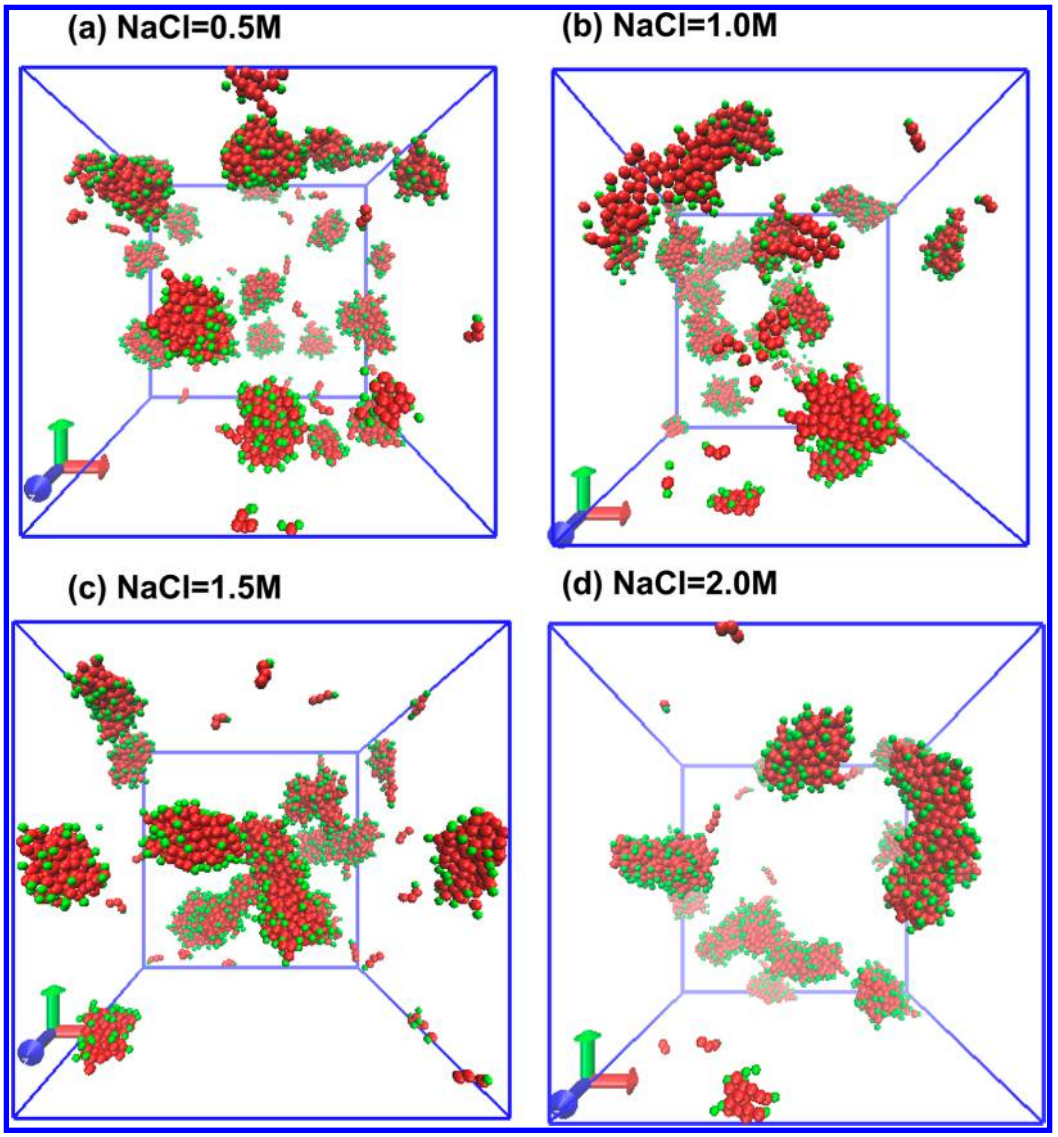

Figure 7. Equilibrated configurations of SDS in the presence of model 1:1 salt C^+A^-. Salt concentrations are (a) 0.5 M, (b) 1 M, (c) 1.5 M, and (d) 2 M. The tail beads are red, and the head beads are green. The surfactant volume fraction is $\phi = 0.04$.

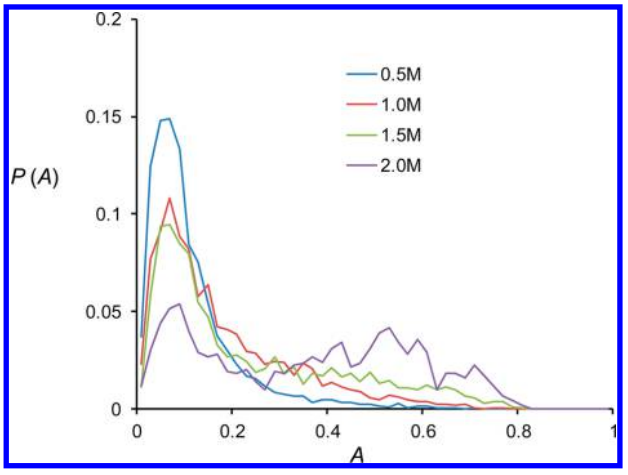

Figure 8. Distribution of the asphericity factors of SDS micelles at different salt concentrations. $A = 0$ corresponds to the spherical micelle shape; larger values of A characterize aggregates of elongated shape.

for perfectly spherical micelles and reaches 1 for perfect cylinders. As shown in Figure 8, it is clear that salt addition sharply decreases the fraction of spherical micelles and increases the number of elongated micelles at 0.5 and 1 M salt concentrations. In 2 M salt solution, the asphericity factor distributions show a well-defined peak corresponding to cylindrical micelles. The limited system size does not allow one to identify the aggregation transition, but worm-like micelles become visually prominent between 0.5 and 1 M. In experiment,[44,45] the transition to worm-like micelles at a similar surfactant volume fraction ϕ occurs when the salt concentration reaches 0.6 M.

6. AGGREGATION IN CATANIONIC SURFACTANT MIXTURES

Mixtures of cationic and anionic surfactants are of specific practical interest, as they are widely used in surfactant formulations.[48] When an oppositely charged surfactant is incorporated into a micelle, the overall micelle charge decreases. The reduced charge weakens the repulsion between the ionic heads in the micelle corona, thus decreasing the

DOI: 10.1021/acs.jpcb.5b05630
J. Phys. Chem. B XXXX, XXX, XXX−XXX

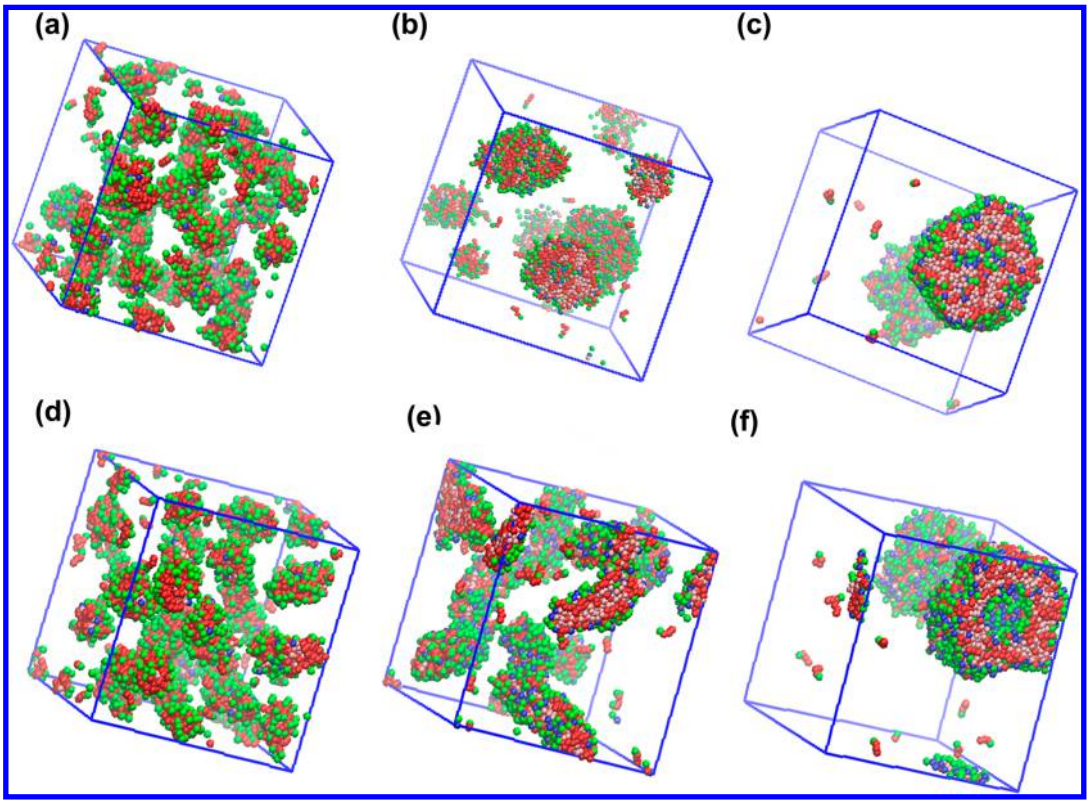

Figure 9. Equilibrated configurations of micelles in SDS−CTAB mixtures of different composition (total surfactant volume fraction ϕ_{total} = 0.08) obtained with different head−water repulsion parameters a_{HW}: (a−c) $a_{HW} = 106.5k_BT/R_c$; (d−f) $a_{HW} = 96.5k_BT/R_c$. (a and d) 9/1 SDS−CTAB mixture. (b and e) 2/1 SDS−CTAB mixture. (c and f) 1/1 SDS−CTAB mixture. The red beads and pink beads are SDS and CTAB tail beads, while green beads and blue beads are SDS and CTAB head beads, respectively.

chemical potential of surfactant molecules in the micelles and lowering the concentration of the free surfactant. A lower charge of the micelle surface causes an increase of the surface density of the heads in the corona. Therefore, as the fraction of oppositely charged surfactant grows, the spherical micelles elongate, adopt a quasi-cylindrical shape, and then turn into unilamella vesicles or multilamella formations.[49] Lamella formation is most typical when the micelle charge approaches zero, that is, close to 1:1 surfactant ratio. Experimental studies of the morphology of catanionic surfactant mixtures are very limited. SDS-DTAB (dodecyltrimethylammonium bromide) mixture was studied by Henderson et al.[49] At constant surfactant volume fractions between ϕ = 0.02 and ϕ = 0.05, vesicles start to form. When the DTAB/SDS ratio reaches 35/65, the transition to vesicles is preceded by the formation of worm-like micelles. When the DTAB/SDS ratio exceeds approximately 40/60, vesicles are in equilibrium with a bulk precipitate.[49] It should also be noted that the behavior of such mixtures is very complex and the phase diagram boundaries are not really precise. For example, an earlier cryo-TEM study by Kamenka et al.[50] revealed coexistence of worm-like micelles, multilamella vesicles, and unilamella vesicles in the same SDS/DTAB sample. This behavior cannot be reproduced in a relatively small DPD box and probably is not entirely reproducible in experiments.[50]

We performed simulations of SDS−CTAB mixtures at constant ϕ = 0.08 and three SDS/CTAB molar ratios—9/1, 2/1, and 1/1—with the interaction parameters from Table 1. Figure 9a shows a snapshot of the surfactant configuration for the 9/1 SDS/CTAB mixture. Addition of CTAB causes elongation of micelles that tend to adopt a worm-like shape. As the SDS/CTAB ratio decreases to 2/1, the micelle configuration drastically changes, with a substantial decrease in the average asphericity factor from 0.11 in 9/1 mixture to 0.05. Instead of the cylindrical aggregates, we observe spheroidal shell-like micelles with ionic heads located both outside and inside the aggregates, as shown in Figure 9b. The inner part of the shell-like micelles contains a certain amount of solvent. The shell-like micelles are very small vesicles, but interestingly, the shell-like micelles never merge or form a single bilayer. Such morphological stability makes shell-like micelles suitable as drug delivery vehicles.

The free surfactant concentration drops dramatically compared to pure SDS even for the 9/1 mixture, and it is barely detectable for the 2/1 mixture. If the fraction of CTAB increases further to a 1/1 ratio, the shell-like vesicles merge and a phase separation occurs onto water and amphiphile-rich phases. The latter has an irregular structure and processes a substantial share of water inclusions, as shown in Figure 9c. This phase separation reflects surfactant precipitation that is similar to the experimental observations.[49,50] Making an exact analogy to these observations is rather difficult, because the precipitate in experiment often contains surfactant crystal-hydrates, that is not captured in the soft-core DPD models. Overall, the DPD model reproduces general qualitative features of the surfactant precipitation phenomenon, but the quantitative deviations from the experimental behavior are quite substantial.

While the short-range repulsion parameter a_{HW} barely influences the CMC for pure SDS, it affects substantially the segregation morphology as the concentration of CTAB increases. Figure 9d−f shows the structural evolution of the

DOI: 10.1021/acs.jpcb.5b05630
J. Phys. Chem. B XXXX, XXX, XXX−XXX

same system with a reduced head−water repulsion parameter a_{HW} = 96.5 k_BT/R_c (instead of a_{HW} = 106.5 k_BT/R_c). A smaller value of a_{HW} makes head−water interactions more favorable than head−head or water−water interactions. In the 9/1 SDS/CTAB mixture, we observe spheroidal aggregates (Figure 9d). Further increase of CTAB fraction to 2/1 leads to a well-defined cylindrical structure that is transformed into a unilamella morphology at 1/1 mixture. The model with a_{HW} = 96.5 k_BT/R_c seems to give reasonable agreement with experiment as far as the morphology evolution is concerned. However, the absence of an independent parametrization method for the interactions between hydrophilic components, in particular, between heads and water, limits predictive capabilities of the proposed coarse-grained model to a qualitative level.

7. CONCLUSIONS

In this paper, we examine the capabilities of the smeared charge model within the standard DPD simulation scheme for studies of micellization of ionic surfactants. We explore several featured characteristics for ionic surfactants: (1) nonmonotonic dependence of the free surfactant concentration on the total concentration, (2) salt effect on the aggregation morphology, and (3) transformation of micellar morphology in the mixtures of ionic and anionic surfactants. As a case study system, we consider the common industrial surfactants CTAB and SDS, the coarse-grained models of which are carefully parameterized on the basis of a combination of atomistic molecular simulations and infinite dilution activity coefficient calibration.

Overall, the proposed model reproduces the qualitative features of ionic surfactant systems fairly well. We correctly reproduce the decrease in the free surfactant concentrations C_f with the overall concentration C_T after the latter exceeds the CMC, which is a feature specific to ionic surfactants. The decrease of C_f with C_T was recently shown in semiatomistic simulations of Sanders et al.[38] but has not yet been reported in DPD or other coarse-grained simulations. A substantial difference in CMC values determined from the free micelle concentration C_f and the premicellar concentration, which was obtained by LeBard et al.[51] in hard-core coarse grained MD, indicated a similar correlation between C_f and C_T. Sanders et al.[38] also noticed that the degree of dissociation between the micelle-forming surfactant and the counterion is important and should be taken into account when micellar solutions of ionic surfactants are considered. The soft-core DPD models are unable to account for the degree of dissociation, and the very criteria of dissociation are difficult to establish. However, the fact that the dependence of C_f on C_T well fits a semiempirical model (eq 3), which uses the experimental value of the dissociation degree, is certainly promising.

The salt effect of charge screening achieved by addition of electrolyte is qualitatively reproduced in the proposed DPD model. The simulations manifest the micelle growth and elongation with the added salt concentration, and the location of the spherical-to-wormlike transition appears to correlate well with the experimental data. It is also important that the model qualitatively describes the structure of the anionic and cationic surfactant mixtures: the transition from cylindrically shaped micelles to vesicle-like aggregates occurs as the total charge of the system decreases.

It is worth noting that, while the proposed DPD model is capable of qualitative description of nontrivial behavior of ionic surfactant solutions, its quantitative ability is limited. The model overestimated the CMC for both SDS and CTAB solutions by a factor of 2−3. This discrepancy is not that large, considering the state of the art in DPD simulations of electrolytes. The reason for this discrepancy is not yet clear, and may be related to the short-range repulsion parameters, which the CMC is extremely sensitive to. At the same time, the model underestimates the micelle size. We hypothesize that this deficiency is related to the isotropic charge distribution around the ionic group and uniform dielectric constant. As a result, the energy of interactions between two charged beads does not depend on the environment. Two charged beads in the micelle corona interact identically to a pair of ions separated by the same distance and immersed in a water bath. The other issue is the inability of the DPD model to account for dissociation and recombination of ionic heads and their counterions. It is possible that the dissociation degree for ionic groups in the micelle coronas is artificially inflated, effectively increasing the local charge and thus strengthening the electrostatic repulsion between the heads, that causes smaller micelle size and larger CMC. We suspect that these problems are inherent not only to the DPD smeared charge model employed here but to all coarse grained models that imply a uniform dielectric medium. The simplicity of the water model, which is represented by beads with isotropic interactions and uniform dielectric constant, does not allow for accounting for the changes in the water structure near the micelle surface caused by hydrophobic and electrostatic interactions. This deficiency may be overcome by polarizable water models for DPD, which have been recently introduced by Peter et al.[52,53]

This study shows the directions for further development and refinement of the DPD models of ionic systems. There is a lack of methods for specific parametrization of the charged beads; both the repulsive parameters and the electrostatic interaction parameters, such as the effective smearing lengths, are currently considered to be independent of the charge group type. For example, a larger λ value for S^- and a smaller λ for N^+ in eq 2 seem to be appropriate considering the electron distributions in sulfate and tetraalkylammonium groups. Currently, the choice of λ is based on technical considerations rather than on special physical criteria, which is an apparent shortcoming of the current model. Let us assume that instead of SDS we would have to develop a model for dodecyltrimethylammonium chloride (DTACl). The only differences from the SDS model would be the opposite charges of the head ($+e$ instead of $-e$) and the counterion (vice versa) and slightly different head−tail bond rigidities, which would hardly affect the values of the CMC and N_{ag} in DPD simulations. However, the experimental CMC of DTACl is about 20 mM,[54] which is 2.2 times higher than that for SDS and is very close to our DPD result (19 mM). The current DPD models of counterions simply do not distinguish between Cl^- and Br^- counterions, but experimental CMCs do differ (DTAB has a CMC of 14−15 mM,[55] lower than DTACl). A similar problem was faced in the simulations of hydrated metal-substituted Nafion:[30] the properties of Nafion polymer significantly depend on the counterion type, but the DPD model does not account for that. Our results show that the shape of aggregates and the conditions of morphological transitions in catanionic mixtures are very sensitive to the parameters of interactions between the ionic groups and the solvent. This effect is expected, since as the overall surface charge of the aggregates decreases, the conservative repulsive interactions start to play a key role affecting the system behavior. Even with refined conservative

DOI: 10.1021/acs.jpcb.5b05630
J. Phys. Chem. B XXXX, XXX, XXX−XXX

parameters, the current DPD model cannot reproduce the experimental phase diagram for the SDS−DTAB−water system that is strongly asymmetric: the micellar morphologies in DTAB-rich mixtures are not the same as those in SDS-rich mixtures with the inverse SDS/DTAB ratios. It is likely that modification of electrostatic contributions or introduction of a special "association" term is required to reproduce the asymmetry.

Despite the deficiencies discussed above, we conclude that the DPD model with smeared charge electrostatic potentials represents a significant advancement in the coarse-grained modeling of ionic systems. The rigorous parametrization of the intracomponent and intercomponent soft repulsive potentials and nearest neighbor and second neighbor bond potentials secures the reproducibility of the basic thermodynamic (solubility) and conformational (chain rigidity) properties. The ability of qualitative description of such complex phenomena like micellization of cationic and anionic surfactants, salt effect, and morphological transitions in catanionic mixtures makes the proposed model a promising tool for studies of self-assembly and thermodynamics in complex soft matter systems including multicomponent electrolyte solutions, polyelectrolyte membranes, and biopolymers.

■ ASSOCIATED CONTENT

Supporting Information

The Supporting Information is available free of charge on the ACS Publications website at DOI: 10.1021/acs.jpcb.5b05630.

Details of MD simulations for fitting the bond parameters (section S1), choice of the electrostatic parameters (section S2), choice of system size and equilibration period (section S3), and choice of n_{mono} and n_{mic} (section S4) (PDF)

■ AUTHOR INFORMATION

Corresponding Author

*Phone: +1-848-445-0834. E-mail: aneimark@rutgers.edu.

Notes

The authors declare no competing financial interest.

■ ACKNOWLEDGMENTS

The authors thank Dr. Minerva Gonzalez Melchor for her useful correspondence. This work is supported by NSF grant DMR-1207239 and DTRA grant HDTRA1-14-1-0015.

■ REFERENCES

(1) Hoogerbrugge, P. J.; Koelman, J. Simulating Microscopic Hydrodynamic Phenomena With Dissipative Particle Dynamics. *Europhys. Lett.* **1992**, *19* (3), 155−160.

(2) Boek, E. S.; Coveney, P. V.; Lekkerkerker, H. N. W.; Vanderschoot, P. Simulating The Rheology of Dense Colloidal Suspensions Using Dissipative Particle Dynamics. *Phys. Rev. E: Stat. Phys., Plasmas, Fluids, Relat. Interdiscip. Top.* **1997**, *55* (3), 3124−3133.

(3) Groot, R. D.; Madden, T. J. Dynamic Simulation of Diblock Copolymer Microphase Separation. *J. Chem. Phys.* **1998**, *108* (20), 8713−8724.

(4) Spenley, N. A. Scaling Laws For Polymers In Dissipative Particle Dynamics. *Europhys. Lett.* **2000**, *49* (4), 534−540.

(5) Groot, R. D.; Rabone, K. L. Mesoscopic Simulation of Cell Membrane Damage, Morphology Change and Rupture by Nonionic Surfactants. *Biophys. J.* **2001**, *81* (2), 725−736.

(6) Prinsen, P.; Warren, P. B.; Michels, M. A. J. Mesoscale Simulations of Surfactant Dissolution and Mesophase Formation. *Phys. Rev. Lett.* **2002**, *89* (14), 148302.

(7) Groot, R. D.; Warren, P. B. Dissipative Particle Dynamics: Bridging the Gap Between Atomistic and Mesoscopic Simulation. *J. Chem. Phys.* **1997**, *107* (11), 4423−4435.

(8) Dorenbos, G. Dependence of Pore Morphology and Diffusion on Hydrophilic Site Distribution within Hydrated Amphiphilic Multi Block Co-Polymer Membranes. *Polymer* **2013**, *54* (18), 5024−5034.

(9) Wu, D.; Paddison, S. J.; Elliott, J. A.; Hamrock, S. J. Mesoscale Modeling of Hydrated Morphologies of 3M Perfluorosulfonic Acid-Based Fuel Cell Electrolytes. *Langmuir* **2010**, *26* (17), 14308−14315.

(10) Yamamoto, S.; Hyodo, S. A. A Computer Simulation Study of the Mesoscopic Structure of The Polyelectrolyte Membrane Nafion. *Polym. J. (Tokyo, Jpn.)* **2003**, *35* (6), 519−527.

(11) Kyrylyuk, A. V.; Fraaije, J. Microphase Separation of Weakly Charged Block Polyelectrolyte Solutions: Donnan Theory for Dynamic Polymer Morphologies. *J. Chem. Phys.* **2004**, *121* (6), 2806−2812.

(12) Yang, S.; Vishnyakov, A.; Neimark, A. V. Self-Assembly in Block Polyelectrolytes. *J. Chem. Phys.* **2011**, *134* (5), 054104.

(13) Groot, R. D. Electrostatic Interactions in Dissipative Particle Dynamics-Simulation of Polyelectrolytes and Anionic Surfactants. *J. Chem. Phys.* **2003**, *118* (24), 11265−11277.

(14) Gonzalez-Melchor, M.; Mayoral, E.; Velazquez, M. E.; Alejandre, J. Electrostatic Interactions in Dissipative Particle Dynamics Using The Ewald Sums. *J. Chem. Phys.* **2006**, *125* (22), 224107.

(15) Warren, P. B.; Vlasov, A.; Anton, L.; Masters, A. J. Screening Properties of Gaussian Electrolyte Models, with Application To Dissipative Particle Dynamics. *J. Chem. Phys.* **2013**, *138* (20), 204907.

(16) Warren, P. B.; Vlasov, A. Screening Properties of Four Mesoscale Smoothed Charge Models, with Application To Dissipative Particle Dynamics. *J. Chem. Phys.* **2014**, *140* (8), 084904.

(17) Posel, Z.; Limpouchová, Z.; Šindelka, K.; Lísal, M.; Procházka, K. Dissipative Particle Dynamics Study of The Ph-Dependent Behavior of Poly(2-Vinylpyridine)-Block-Poly(Ethylene Oxide) Diblock Copolymer in Aqueous Buffers. *Macromolecules* **2014**, *47* (7), 2503−2514.

(18) Yang, K.; Vishnyakov, A.; Neimark, A. V. Polymer Translocation through a Nanopore: DPD Study. *J. Phys. Chem. B* **2013**, *117* (13), 3648−3658.

(19) Wang, Y.-L.; Lu, Z.-Y.; Laaksonen, A. Specific Binding Structures of Dendrimers on Lipid Bilayer Membranes. *Phys. Chem. Chem. Phys.* **2012**, *14* (23), 8348−8359.

(20) Vishnyakov, A.; Talaga, D. S.; Neimark, A. V. DPD Simulation of Protein Conformations: From Alpha-Helices to Beta-Structures. *J. Phys. Chem. Lett.* **2012**, *3* (21), 3081−3087.

(21) Ibergay, C.; Malfreyt, P.; Tildesley, D. J. Electrostatic Interactions In Dissipative Particle Dynamics: Toward A Mesoscale Modeling of The Polyelectrolyte Brushes. *J. Chem. Theory Comput.* **2009**, *5* (12), 3245−3259.

(22) Cheong, D. W.; Panagiotopoulos, A. Z. Monte Carlo Simulations of Micellization in Model Ionic Surfactants: Application to Sodium Dodecyl Sulfate. *Langmuir* **2006**, *22* (9), 4076−4083.

(23) Jusufi, A.; Hynninen, A.-P.; Panagiotopoulos, A. Z. Implicit Solvent Models For Micellization of Ionic Surfactants. *J. Phys. Chem. B* **2008**, *112* (44), 13783−13792.

(24) Martin, T. J.; Prochazka, K.; Munk, P.; Webber, S. E. pH-Dependent Micellization of Poly(2-Vinylpyridine)-Block-Poly-(Ethylene Oxide). *Macromolecules* **1996**, *29* (18), 6071−6073.

(25) Sindelka, K.; Limpouchova, Z.; Lisal, M.; Prochazka, K. Dissipative Particle Dynamics Study of Electrostatic Self-Assembly in Aqueous Mixtures of Copolymers Containing One Neutral Water-Soluble Block and One Either Positively or Negatively Charged Polyelectrolyte Block. *Macromolecules* **2014**, *47* (17), 6121−6134.

(26) Vishnyakov, A.; Lee, M.-T.; Neimark, A. V. Prediction of The Critical Micelle Concentration of Nonionic Surfactants by Dissipative Particle Dynamics Simulations. *J. Phys. Chem. Lett.* **2013**, *4* (5), 797−802.

DOI: 10.1021/acs.jpcb.5b05630
J. Phys. Chem. B XXXX, XXX, XXX−XXX

(27) Jorn, R.; Voth, G. A. Mesoscale Simulation of Proton Transport in Proton Exchange Membranes. *J. Phys. Chem. C* **2012**, *116* (19), 10476−10489.
(28) Fuchslin, R. M.; Fellermann, H.; Eriksson, A.; Ziock, H.-J. Coarse Graining and Scaling in Dissipative Particle Dynamics. *J. Chem. Phys.* **2009**, *130* (21), 214102.
(29) Lee, M.-T.; Vishnyakov, A.; Neimark, A. V. Calculations of Critical Micelle Concentration by Dissipative Particle Dynamics Simulations: The Role of Chain Rigidity. *J. Phys. Chem. B* **2013**, *117* (35), 10304−10310.
(30) Cheng, J. L.; Vishnyakov, A.; Neimark, A. V. Morphological Transformations in Polymer Brushes in Binary Mixtures: DPD Study. *Langmuir* **2014**, *30* (43), 12932−12940.
(31) Ewald, P. P. Evaluation of optical and electrostatic lattice potentials. *Ann. Phys.* **1921**, *64*, 253−287.
(32) Mackerell, A. D.; Banavali, N.; Foloppe, N. Development and Current Status of The CHARMM Force Field For Nucleic Acids. *Biopolymers* **2000**, *56*, 257−265.
(33) Widom, B. Some Topics in the Theory of Fluids. *J. Chem. Phys.* **1963**, *39*, 2808−2812.
(34) Seaton, M. A.; Anderson, R. L.; Metz, S.; Smith, W. DL_MESO: Highly Scalable Mesoscale Simulations. *Mol. Simul.* **2013**, *39* (10), 796−821.
(35) Johnson, I.; Olofsson, G.; Jonsson, B. Micelle Formation of Ionic Amphiphiles - Thermochemical Test of a Thermodynamic Model. *J. Chem. Soc., Faraday Trans. 1* **1987**, *83*, 3331−3344.
(36) Polacek, R.; Kaatze, U. Monomer Exchange Kinetics, Radial Diffusion, and Hydrocarbon Chain Isomerization of Sodium Dodecylsulfate Micelles In Water. *J. Phys. Chem. B* **2007**, *111* (7), 1625−1631.
(37) Quina, F. H.; Nassar, P. M.; Bonilha, J. B. S.; Bales, B. L. Growth of Sodium Dodecyl-Sulfate Micelles with Detergent Concentration. *J. Phys. Chem.* **1995**, *99* (46), 17028−17031.
(38) Sanders, S. A.; Sammalkorpi, M.; Panagiotopoulos, A. Z. Atomistic Simulations of Micellization of Sodium Hexyl, Heptyl, Octyl, and Nonyl Sulfates. *J. Phys. Chem. B* **2012**, *116* (8), 2430−2437.
(39) Anachkov, S. E.; Danov, K. D.; Basheva, E. S.; Kralchevsky, P. A.; Ananthapadmanabhan, K. P. Determination of The Aggregation Number and Charge of Ionic Surfactant Micelles from the Stepwise Thinning of Foam Films. *Adv. Colloid Interface Sci.* **2012**, *183*, 55−67.
(40) Sepulveda, L.; Cortes, J. Ionization Degrees and Critical Micelle Concentrations of Hexadecyltrimethylammonium and Tetradecyltrimethylammonium Micelles with Different Counterions. *J. Phys. Chem.* **1985**, *89* (24), 5322−5324.
(41) Benrraou, M.; Bales, B. L.; Zana, R. Effect of The Nature of the Counterion on the Properties of Anionic Surfactants. 1. CMC, Ionization Degree at the CMC and Aggregation Number of Micelles of Sodium, Cesium, Tetramethylammonium, Tetraethylammonium, Tetrapropylammonium, and Tetrabutylammonium Dodecyl Sulfates. *J. Phys. Chem. B* **2003**, *107* (48), 13432−13440.
(42) Weidemaier, K.; Tavernier, H. L.; Fayer, M. D. Photoinduced Electron Transfer on The Surfaces of Micelles. *J. Phys. Chem. B* **1997**, *101* (45), 9352−9361.
(43) Lianos, P.; Zana, R. Fluorescence Probe Studies of The Effect of Concentration on The State of Aggregation of Surfactants in Aqueous-Solution. *J. Colloid Interface Sci.* **1981**, *84* (1), 100−107.
(44) Mazer, N. A.; Benedek, G. B.; Carey, M. C. An Investigation of The Micellar Phase of Sodium Dodecyl Sulfate in Aqueous Sodium Chloride Solutions Using Quasielastic Light Scattering Spectroscopy. *J. Phys. Chem.* **1976**, *80* (10), 1075−1085.
(45) Berr, S. S.; Jones, R. R. Effect of Added Sodium and Lithium Chlorides on Intermicellar Interactions and Micellar Size of Aqueous Dodecyl Sulfate Aggregates as Determined by Small-Angle Neutron Scattering. *Langmuir* **1988**, *4* (6), 1247−1251.
(46) Sammalkorpi, M.; Karttunen, M.; Haataja, M. Ionic Surfactant Aggregates in Saline Solutions: Sodium Dodecyl Sulfate (SDS) In the Presence of Excess Sodium Chloride (NaCl) or Calcium Chloride ($CaCl_2$). *J. Phys. Chem. B* **2009**, *113* (17), 5863−5870.
(47) Rudnick, J.; Gaspari, G. The Asphericity of Random Walks. *J. Phys. A: Math. Gen.* **1986**, *19* (4), L191.
(48) Kume, G.; Gallotti, M.; Nunes, G. Review on Anionic/Cationic Surfactant Mixtures. *J. Surfactants Deterg.* **2008**, *11* (1), 1−11.
(49) Herrington, K. L.; Kaler, E. W.; Miller, D. D.; Zasadzinski, J. A.; Chiruvolu, S. Phase Behavior of Aqueous Mixtures of Dodecyltrimethylammonium Bromide (DTAB) and Sodium Dodecyl Sulfate (SDS). *J. Phys. Chem.* **1993**, *97* (51), 13792−13802.
(50) Kamenka, N.; Chorro, M.; Talmon, Y.; Zana, R. Study of Mixed Aggregates in Aqueous-Solutions of Sodium Dodecyl-Sulfate and Dodecyltrimethylammonium Bromide. *Colloids Surf.* **1992**, *67*, 213−222.
(51) Lebard, D. N.; Levine, B. G.; Mertmann, P.; Barr, S. A.; Jusufi, A.; Sanders, S.; Klein, M. L.; Panagiotopoulos, A. Z. Self-Assembly of Coarse-Grained Ionic Surfactants Accelerated by Graphics Processing Units. *Soft Matter* **2012**, *8* (8), 2385−2397.
(52) Peter, E. K.; Pivkin, I. V. A Polarizable Coarse-Grained Water Model for Dissipative Particle Dynamics. *J. Chem. Phys.* **2014**, *141* (16), 164506.
(53) Peter, E. K.; Pivkin, I. V.; Shea, J.-E. A kMC-MD Method with Generalized Move-Sets for The Simulation of Folding of Alpha-Helical and Beta-Stranded Peptides. *J. Chem. Phys.* **2015**, *142* (14), 144903.
(54) Bales, B. L.; Zana, R. Characterization of Micelles of Quaternary Ammonium Surfactants, as Reaction Media I: Dodeclytrimethylammonium Bromide and Chloride. *J. Phys. Chem. B* **2002**, *106* (8), 1926−1939.
(55) Bahri, M. A.; Hoebeke, M.; Grammenos, A.; Delanaye, L.; Vandewalle, N.; Seret, A. Investigation of SDS, DTAB and CTAB Micelle Microviscosities by Electron Spin Resonance. *Colloids Surf., A* **2006**, *290* (1−3), 206−212.

DOI: 10.1021/acs.jpcb.5b05630
J. Phys. Chem. B XXXX, XXX, XXX−XXX